The small non-coding vault RNA1-1 acts as a riboregulator of autophagy

Authors: Rastislav Horos[1], Anne-Marie Alleaume[1], Roos Kleinendorst[1], Abul K. Tarafder[1], Thomas Schwarzl[1], Elisabeth M. Zielonka[1], Asli Adak[1], Alfredo Castello[2], Wolfgang Huber[1], Carsten Sachse[1], and Matthias W. Hentze[1]*

Affiliations:

[1]EMBL Heidelberg, Meyerhofstrasse 1, 69117 Heidelberg, Germany

[2]Department of Biochemistry, University of Oxford, South Parks Road, Oxford OX1 3QU, United Kingdom

*Correspondence to: hentze@embl.de

Abstract: Vault RNAs (vtRNA) are small, 88-100nt non-coding RNAs found in many eukaryotes. Although they have been linked to drug resistance, apoptosis and nuclear transport, their function remains unclear. Here we show that a human vtRNA, RNA1-1, specifically binds to the autophagy receptor sequestosome-1/p62. Antisense-mediated depletion of vault RNA1-1 augments, whereas increased vault RNA1-1 expression restricts, autophagic flux in a p62-dependent manner. Bulk autophagy induced by starvation reduces the levels of vault RNA1-1 and the fraction of RNA-bound p62. These findings show that RNAs can act as riboregulators of biological processes by interacting with proteins, and assign a function to a vault RNA.

Main Text: Eukaryotic small non-coding RNAs, such as miRNAs, siRNAs, tRNAs, and snoRNAs, etc., function as scaffolds that recruit protein complexes to complementary RNA sequences. Whether small non-coding RNAs might have additional functions is less clear.

Vault RNAs (vtRNA) are small non-coding RNA components of giant ribonucleoprotein particles termed vaults (*1*). Humans express four vtRNA paralogs (vtRNA1-1, vtRNA1-2, vtRNA1-3, vtRNA2-1), which are 88-100nt long and transcribed by RNA polymerase III. Vaults are found in a broad spectrum of eukaryotes ranging from slime moulds to mammals (*2*). Although vaults can occur at 10,000 to 100,000 particles per cell and have been linked to cellular processes like drug resistance, apoptosis and nuclear transport (*3*), the function of vaults or vault RNAs remains unclear. Sedimentation experiments showed that only a minor fraction of vtRNAs is incorporated into vaults (*4*, *5*), suggesting they may have functions outside of vault complexes.

Autophagy is an essential process responsible for the recognition, removal and degradation of intracellular components, organelles and foreign bodies within membrane vesicles termed autophagosomes (*6*, *7*). Specific receptors including sequestosome-1/p62 bind ubiquitinated cargos and deliver them to autophagosomes by interaction with LC3 proteins (*8*). Subsequently, the autophagosomes enclose and fuse with lysosomes to degrade their contents.

Here we show that the autophagy receptor p62 is an RNA-binding protein that binds vault RNAs. We further demonstrate that vault RNA1-1 can control the autophagic flux via p62 at an early stage in the autophagic pathway. Thus, we have identified vault RNA1-1 as a riboregulator of autophagy.

We recently developed a mass spectrometry-based method for the proteome-wide identification of RNA-interacting peptides in RNA-binding proteins (RBPs), termed RBDmap (*9*). We performed RBDmap on human hepatocellular carcinoma HuH-7 cells and isolated

peptides from both known and previously unknown RBPs (*10*) (**Table S1, Supplementary Materials and Methods**). Among these, we identified a peptide mapping to the zinc finger domain of p62, suggesting that p62 interacts with RNA through this domain. None of the known autophagy receptors have been shown to directly bind RNA (*11*, *12*), and we therefore explored this further.

We verified the p62-RNA interaction by multiple approaches. First, we exposed HuH-7 cells to UV-C light to covalently stabilize direct RNA-protein interactions, and purified crosslinked RNA-binding proteins from lysates using oligo-(dT) coupled beads (*13*). We confirmed the presence of p62 in the isolated RNP complexes by Western blotting (**Fig. 1A**). In a complementary approach, we immunoprecipitated (IP) p62 from UV-treated cells after lysis, followed by radioactive labeling of RNA 5' ends (*14*). We observed a radioactive signal with a molecular weight corresponding to p62 (**Fig. 1B**). RNase treatment of the lysates prior to the IP reduced the heterogeneity in band migration, and confirmed the p62-crosslinked entity as RNA (**Fig. 1B**). Proteomics analysis of the IPs indicated that p62 is the major purified protein at the size of the radioactive signal appearance (**Table S2**). Therefore, p62 is an RNA-binding protein.

To further investigate the p62-RNA interaction, we mutated positively charged or aromatic amino acids within the RNA-binding region implicated by RBDmap (**Fig 1C and D**). We evaluated tagged p62 variants in HuH-7 cells by IP and RNA labeling. We found that substitution of the conserved residue K141 within the zinc finger domain of p62 appeared to decrease RNA binding (**fig. S1A**), however the oligomerization of endogenous wild-type p62 with this p62 variant interfered with the analysis. We depleted endogenous p62 from HuH-7 cells by RNAi and, consistent with the above data, the p62-K141A variant showed a substantial reduction in RNA binding compared to p62-wt. RNA binding was further reduced in the

R139/K141-AA variant (RK/A, **Fig. 1E**). These data corroborate the RBDmap result and suggest that the zinc finger domain of p62 is important for its interaction with RNA *in vivo*.

To identify the RNA targets bound by p62 we performed iCLIP, which identifies RNA-protein contacts through crosslink sites (CS) (*15*). We sequenced RNAs that co-immuno-purified with p62 using two independent antibodies (and the respective controls, **fig. S1B and C**). All four vault RNAs (vtRNAs) were among the high confidence p62 RNA targets, scoring at the top in the CS density analysis (**Table S3**) as well as in the RNA class enrichment analysis, respectively (**fig. S1D**). Differential CS occurrence of individual RNAs isolated from p62 or control IPs, respectively, placed the vtRNAs prominently in the p62 target list (**Fig. 2A, Table S4**). Knock down (KD) of p62 did not affect vtRNAs levels (**fig. S1E and F**), suggesting that p62 does not regulate vtRNAs stability. Thus, p62 binds a restricted set of RNAs with vtRNAs being the top targets, but it does not mediate vtRNAs degradation.

Closer inspection revealed that p62 preferentially interacts with looped regions within the central domains of vtRNAs (**Fig. 2B and fig. S2**). Overexpression of the vtRNA1-1 central domain has previously been shown to confer anti-apoptotic effects independently of vaults (*16*), therefore we further investigated the interaction of p62 with vtRNA1-1. We established a UV crosslinking and electrophoretic mobility shift assay (EMSA) to evaluate the p62-vtRNA1-1 interaction *in vitro*. Incubation of radiolabeled vtRNA1-1 and MBP-tagged p62 led to the formation of labeled, higher molecular weight RNP complexes (**Fig. 2C**). We found that the K141A and RK/A substitutions reduced the formation of these RNP complexes, consistent with the *in vivo* observations. RNase treatment after crosslinking diminished non-specific interactions, resulting in a protected RNA fragment bound to monomeric MBP-p62 (90 kDa) (**Fig. 2C**). The K141A and RK/A substitutions abolished this RNase-resistant RNA fragment. These findings

mirror the analysis of p62 mutants *in vivo*, and suggest that the p62-vtRNA1-1 interaction requires residues within p62 zinc finger domain.

To explore a possible function of the p62-vtRNA1-1 interaction in autophagy, we overexpressed vtRNA1-1 in HuH-7 cells and monitored autophagic flux by assessing LC3B conjugation from LC3B I to LC3B II during autophagosome assembly and p62 levels, reflecting autolysosomal degradation. Increasing vtRNA1-1 levels reduced LC3B conjugation and induced p62 protein accumulation in a dose-dependent manner (**Fig. 3A and S3A**), suggesting decreased autophagic flux. Overexpression of other vault RNAs did not significantly affect the LC3B-II/LC3B-I ratio (**Fig. 3B and S3A**). Treatment with bafilomycine A_1 (BafA), an inhibitor of autophagosome-lysosome fusion that leads to the accumulation of mature autophagosomes, restored the LC3B conjugation ratio in cells overexpressing vtRNA1-1 (**Fig. 3B**). This result suggests that vtRNA1-1 overexpression did not disturb autophagosome turnover but rather restricted autophagic flux. Further, LNA-mediated KD of vtRNA1-1 resulted in a dose-dependent decrease in p62 levels and increased LC3B conjugation (**Fig. 3C and S3B**). Concurrent removal of p62 (**Fig. 3D,** compare lanes 3 and 4 with 1 and 2**)** or BafA treatment (**Fig. 3D,** compare lanes 5 and 6 with 1 and 2**)** restored the LC3B conjugation ratio in vtRNA1-1 KD cells as compared to control cells. These experiments suggest that the removal of vtRNA1-1 did not inhibit autophagosome turnover and that vtRNA1-1 affects early stages of autophagy via p62.

Next, we investigated the role of the p62-vtRNA1-1 interaction during bulk cytosol autophagy induced by amino acid and serum starvation. During bulk autophagy, p62 supports the increased autophagic flux (*17*), and also serves as degradation substrate (*18*). Indeed, cells that are starved in the presence of BafA show pronounced expression and co-localization of

autophagosomal LC3B and p62 (**fig. S4A**). We found that the p62-RNA interaction gradually decreases during 6 hours of starvation and that this reduction is exacerbated by BafA treatment (**Fig. 4A and B**). These data indicate that bulk autophagy decreases the fraction of RNA-bound p62 relative to total p62, and that p62 destined for lysosomal degradation no longer binds RNA. Consistent with this hypothesis, we found that RNA-bound p62 is enriched in the detergent-soluble subcellular fraction and depleted from the vesicular/nuclear and membrane debris fractions (**Fig. 4C**). For p62, these data reveal an anti-correlation between engagement with RNA and engagement with the autophagy apparatus, suggesting that RNA binding interferes with p62's function during autophagosome formation at an early stage of autophagy.

In addition, the levels of vtRNA1-1, but not other vault RNAs, drop significantly in HuH-7 cells after 6 hours of starvation (**Fig. 4D**). The starvation-induced decrease in vtRNA1-1 levels is not a result of co-degradation with p62, because neither the KD of p62 nor the treatment with BafA significantly restored vtRNA1-1 levels (**Fig. 4D**). The decrease in vtRNA1-1 levels correlates with and possibly causes a decrease in the fraction of RNA-bound p62 during starvation-induced autophagy (**fig. S4B**). Of relevance, PolIII transcription at the vtRNA1-1 locus is dynamically controlled by its repressor MAF1, which in turn is activated by starvation (*19*), suggesting that starvation represses the transcription of vtRNA1-1. Thus, bulk autophagy leads to a concurrent decrease in vtRNA1-1 levels and the fraction of p62 associated with RNA.

Here we show that the small non-coding RNA vtRNA1-1 regulates autophagic flux through the autophagy receptor p62, assigning a function to the first member of this enigmatic family of non-coding RNAs described more than 30 years ago (*1*). Future work will address the functions of the interaction of the other members of the vault RNA family with p62. Moreover, it will be illuminating to unravel the mechanistic and structural details of how vtRNA1-1 controls

the function of p62 in autophagy. Riboregulation of protein function may represent a new general paradigm, complementing well-established forms of regulation such as by protein-protein interactions.

References and notes

1. N. L. Kedersha, L. H. Rome, Isolation and characterization of a novel ribonucleoprotein particle: large structures contain a single species of small RNA. *The Journal of cell biology* **103**, 699-709 (1986).
2. P. F. Stadler *et al.*, Evolution of vault RNAs. *Mol Biol Evol* **26**, 1975-1991 (2009).
3. W. Berger, E. Steiner, M. Grusch, L. Elbling, M. Micksche, Vaults and the major vault protein: novel roles in signal pathway regulation and immunity. *Cellular and molecular life sciences : CMLS* **66**, 43-61 (2009).
4. C. Nandy *et al.*, Epstein-barr virus-induced expression of a novel human vault RNA. *J Mol Biol* **388**, 776-784 (2009).
5. L. B. Kong, A. C. Siva, V. A. Kickhoefer, L. H. Rome, P. L. Stewart, RNA location and modeling of a WD40 repeat domain within the vault. *RNA* **6**, 890-900 (2000).
6. V. Sica *et al.*, Organelle-Specific Initiation of Autophagy. *Molecular cell* **59**, 522-539 (2015).
7. D. J. Klionsky *et al.*, Guidelines for the use and interpretation of assays for monitoring autophagy (3rd edition). *Autophagy* **12**, 1-222 (2016).
8. A. Stolz, A. Ernst, I. Dikic, Cargo recognition and trafficking in selective autophagy. *Nature cell biology* **16**, 495-501 (2014).
9. A. Castello *et al.*, Comprehensive Identification of RNA-Binding Domains in Human Cells. *Molecular cell* **63**, 696-710 (2016).
10. B. M. Beckmann *et al.*, The RNA-binding proteomes from yeast to man harbour conserved enigmRBPs. *Nature communications* **6**, 10127 (2015).

11. H. Guo *et al.*, Autophagy supports genomic stability by degrading retrotransposon RNA. *Nature communications* **5**, 5276 (2014).

12. C. Kraft, A. Deplazes, M. Sohrmann, M. Peter, Mature ribosomes are selectively degraded upon starvation by an autophagy pathway requiring the Ubp3p/Bre5p ubiquitin protease. *Nature cell biology* **10**, 602-610 (2008).

13. A. Castello *et al.*, System-wide identification of RNA-binding proteins by interactome capture. *Nature protocols* **8**, 491-500 (2013).

14. A. G. Baltz *et al.*, The mRNA-bound proteome and its global occupancy profile on protein-coding transcripts. *Molecular cell* **46**, 674-690 (2012).

15. I. Huppertz *et al.*, iCLIP: protein-RNA interactions at nucleotide resolution. *Methods* **65**, 274-287 (2014).

16. M. Amort *et al.*, Expression of the vault RNA protects cells from undergoing apoptosis. *Nature communications* **6**, 7030 (2015).

17. G. Bjorkoy *et al.*, p62/SQSTM1 forms protein aggregates degraded by autophagy and has a protective effect on huntingtin-induced cell death. *The Journal of cell biology* **171**, 603-614 (2005).

18. M. H. Sahani, E. Itakura, N. Mizushima, Expression of the autophagy substrate SQSTM1/p62 is restored during prolonged starvation depending on transcriptional upregulation and autophagy-derived amino acids. *Autophagy* **10**, 431-441 (2014).

19. A. Orioli, V. Praz, P. Lhote, N. Hernandez, Human MAF1 targets and represses active RNA polymerase III genes by preventing recruitment rather than inducing long-term transcriptional arrest. *Genome Res* **26**, 624-635 (2016).

Acknowledgments: The sequencing data were deposited in Array Express with the accession number E-MTAB-4894. This work was supported by a European Research Council Advanced Grant and by a grant from the Virtual Liver Consortium (German Ministry for Education and Research) (to M.W.H.). We are grateful to Bernd Fischer (German Cancer Research Center, Heidelberg, Germany) for the analysis of the RBDmap dataset, to Bernd Klaus (Centre for Statistical Data Analysis, EMBL) for help with statistical analyses, to Charles Girardot (Genome Biology Computational Support, EMBL) for help with sequencing data deposition, to Mandy Rettel (Proteomics facility, EMBL) for proteomic analyses, and to members of the Hentze group for critical reading of the manuscript. The authors declare no competing financial interests.

Fig. 1. The autophagy receptor sequestosome-1/p62 is an RNA-binding protein.

(**A**) Western blot analysis of input and eluate samples from interactome capture experiment. TDP43 serves as a positive control for RNA binding, whereas actin serves as negative control. (**B**) Lysates from UV treated or control cells were treated with dilutions of RNaseA and used for immunoprecipitation followed by radioactive labeling and Western blotting. (**C**) RBDmap-enriched peptide (grey) and a peptide not enriched in the RNA-bound fraction (black) positioned on the p62 protein. The X-axis is scaled to protein length. A scheme of the p62 domain architecture is drawn below. NLS, nuclear localization signal; NES, nuclear export signal, LIR, LC3 interaction region; KIR, Keap1 interaction region; UBA, ubiquitin associated domain. (**D**) Human p62 protein region between AA 101-163. Orthologous proteins are aligned below; dotted region represents insertion of longer peptide. The RBDmap-enriched peptide (FDR 1%) is shaded in grey. *Hs*, *Homo sapiens*, *Mm*, *Mus musculus*, *Xl*, *Xenopus laevis*, *Dr*, *Dario rerio*. (**E**) HuH-7 cells treated with indicated siRNA were transfected with empty vector (ev) or p62 wt and variants (K141A, RK/A refers to the R139/K141-AA). Cells were exposed to 254nm UV-C light, lysed and used for IP followed by the radioactive labeling of RNAs and Western blotting.

Fig. 2. p62 binds vault RNA1-1.

(**A**) Volcano plot of genomic regions with differential CS occurrences. The data were normalized for background, and CS enrichment in p62 IPs over controls was tested with DEseq2. The black dots indicate genomic regions (exons, introns) significantly enriched in p62 IPs (p-adj < 0.05). The open circles indicate vault RNAs. (**B**) Significant (FDR 5%) CS read counts of p62 IPs displayed on the vtRNA1-1 transcript sequence. RNA secondary structure is displayed next to the plot and nucleotides with CS mean count values above 5 are indicated in bold. (**C**) Denaturing EMSA using ^{32}P-UTP labeled vtRNA1-1 with MBP tag only, MBP-p62 wt or MBP-

p62 variant proteins (RK/A refers to the double R139/K141-AA mutant). RNase treatment after the reaction is indicated. Open arrow indicates vtRNA1-1-p62 complex, while the filled arrow indicates RNase-protected fragments at single MBP-p62 unit. * indicates a non-specific band.

Fig. 3. vtRNA1-1 regulates autophagy via p62.

(**A**) HuH-7 cells were transfected with empty vector (ctrl) or increasing amount of vector encoding vtRNA1-1 and lysed after 24 hours. Lysates were analyzed by Western blot with the indicated antibodies. (**B**) Cells were transfected with indicated vtRNAs, vehicle treated or treated with BafA at 100 nM for 5 hours, and then lysed. Lysates were analyzed by Western blotting and images of LC3B staining were quantified. n=3, *** $p<0.005$ (**C**) Cells were transfected with a control LNA oligo (negA), or with increasing amounts of LNA oligos targeting vtRNA1-1, and lysed after 48 hours. Lysates were analyzed by Western blot with the indicated antibodies. (**D**) Cells were transfected with indicated LNA oligos and control or p62 siRNA and incubated for 48 hours. Where indicated, cells were treated with BafA. Lysates were analyzed by Western blotting with the indicated antibodies.

Fig. 4. Starvation reduces p62 RNA binding and vtRNA1-1 expression.

(**A**) Cells were starved in minimal medium containing solvent control or BafA at 100 nM for the indicated time, 254nm UV-C light exposed and lysed. Lysates were used for p62 IP and RNA radiolabeling assay. After SDS-PAGE and transfer, the membrane was exposed overnight on film and used subsequently for Western blotting. (**B**) Phosphorimages and Western blots of 3 independent replicates as described in (A) were used for quantification and ratio calculation (radioactive/IP Western blotting signal). n=3, * $p<0.05$, *** $p< 0.005$ (**C**) HuH-7 cells were exposed to 254 nm UV-C light and lysed in hypotonic buffer. A nuclear and vesicular fraction (N/V) was collected, followed by the pelleting of membranous debris (M). Both pellets and the

supernatant (S) were then used for p62 IP and RNA radiolabeling assay. (**D**) HuH-7 cells were treated with a scrambled control siRNA (Scr) or p62 siRNA for 48 hours, followed by starvation for 6 hours. Total RNA was isolated and analyzed by Northern blotting; phosphorimages were quantified and normalized with the tRNA $Gln^{CUG(3\text{-}2)}$ to the 0 hour time point, n=3, * $p<0.05$, ** $p<0.01$, *** $p< 0.005$

Supplementary Materials

Materials and Methods

References

Tables S1-S4

Figures S1-S4

Figure 1

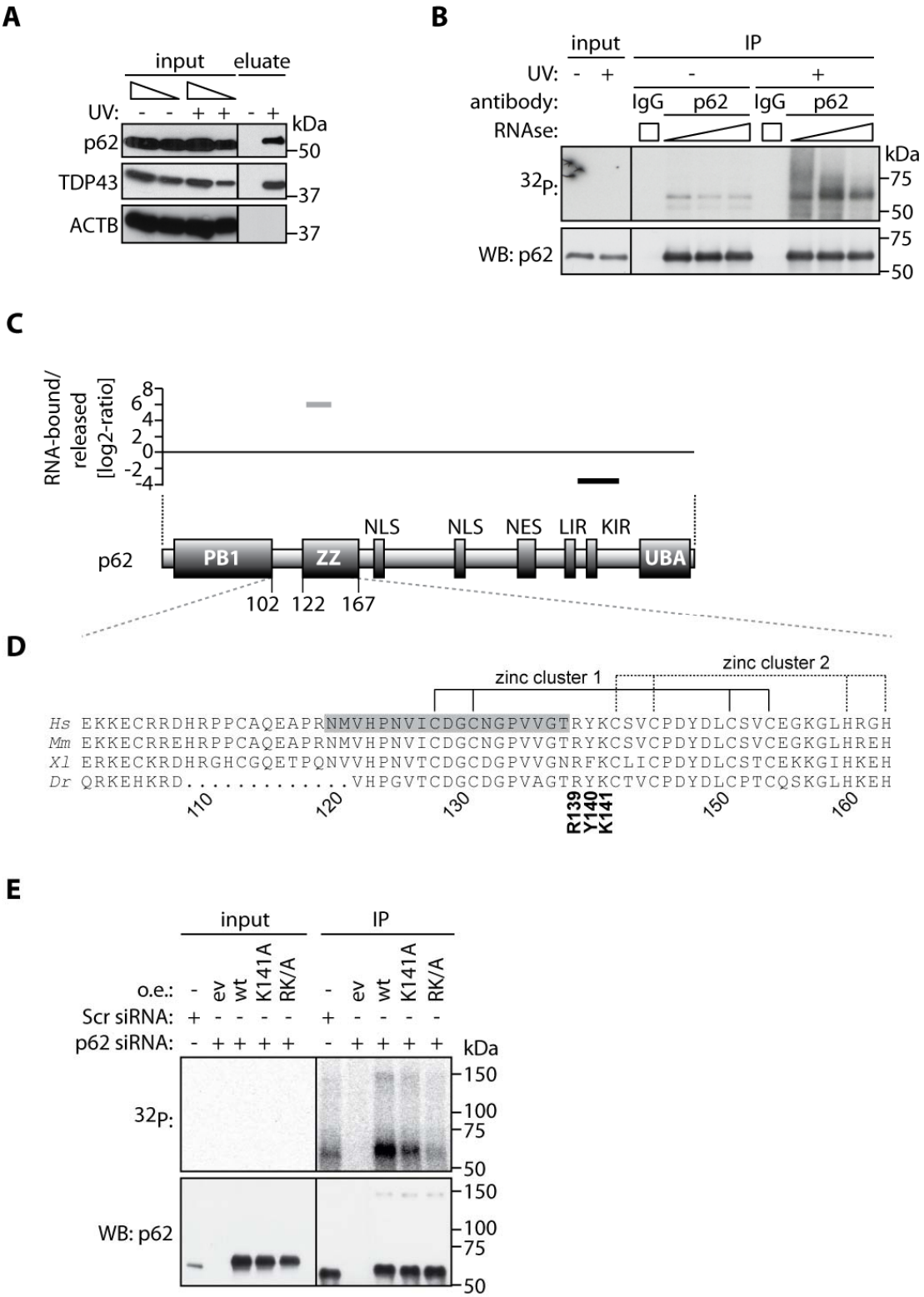

Figure 2

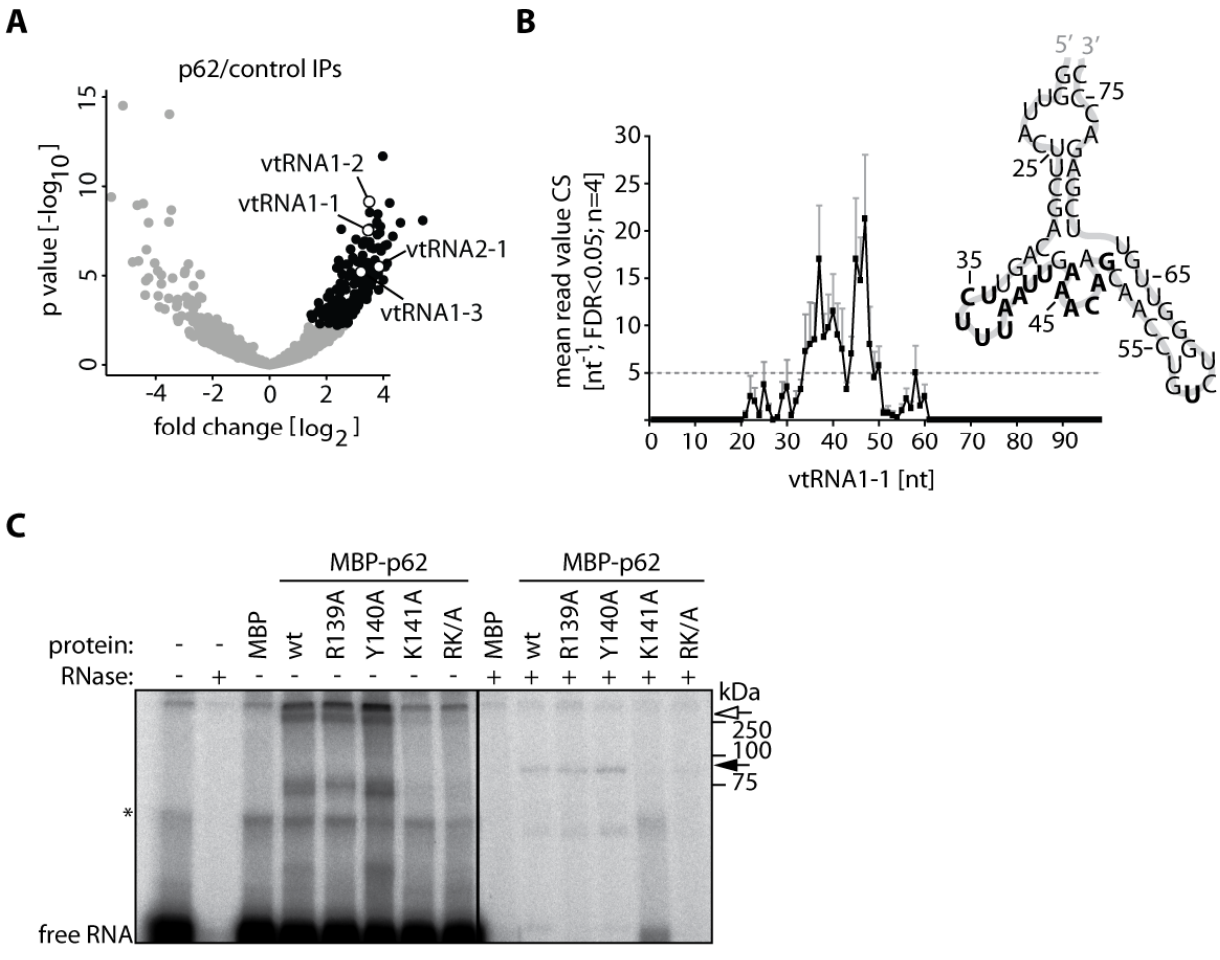

Figure 3

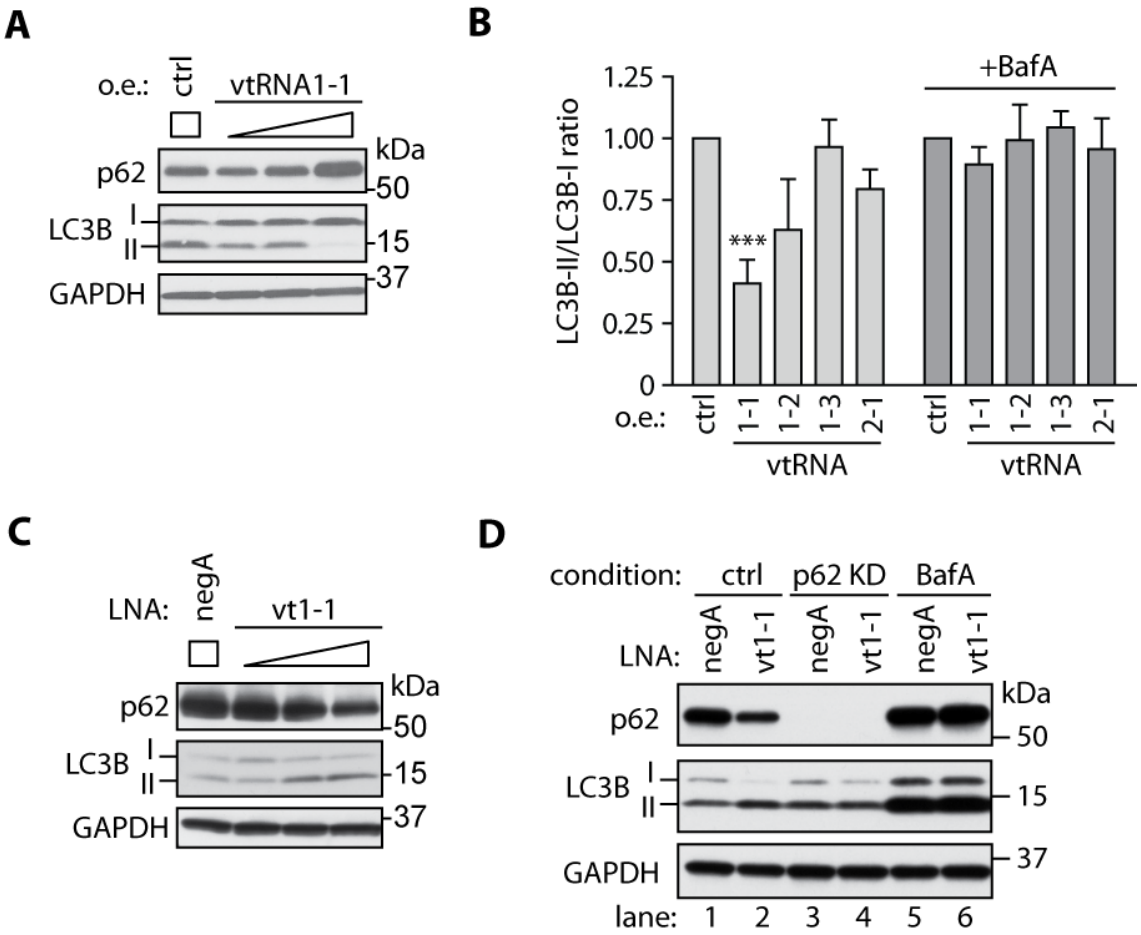

Figure 4

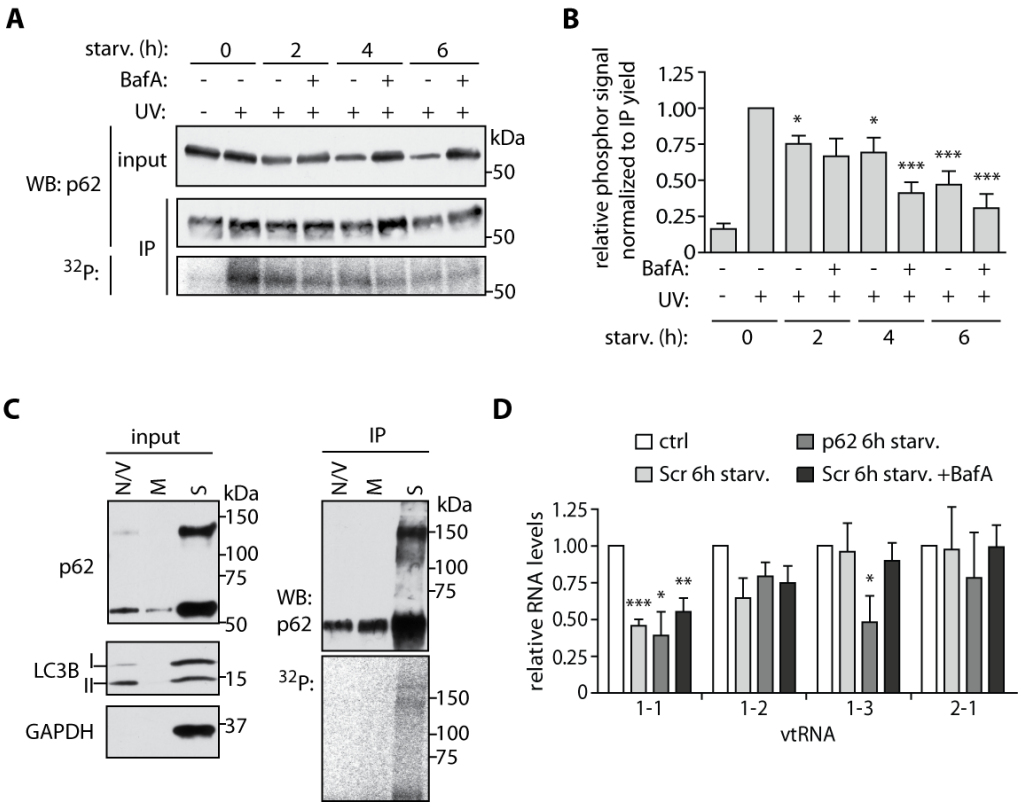

The small non-coding vault RNA1-1 acts as a riboregulator of autophagy

Horos et al.

Supplementary Material

Materials and Methods

Cell culture and chemicals

HuH-7 cells were cultured in low glucose (5mM) DMEM supplemented with 10% heat inactivated FCS (PAA), 2mM L-glutamine (25030081, Thermo Fisher) and 100 U/ml PenStrep (15140122, Thermo Fisher). We derived a HuH-7 Flp-In TREx cell line using published protocols (Flp-In T-Rex, Thermo Fisher), and prepared stably expressing doxycycline-inducible cell lines following manufacturer's instructions. Stable cell lines were grown in medium containing blasticidine (5µg/ml) and zeocin (100 µg/ml) or hygromycin (200 µg/ml). Induction was performed with doxycycline at 100 ng/ml overnight. Transfections were done using Lipofectamine 3000 (L3000008, Thermo Fisher) for the plasmids, or Lipofectamine RNAiMax (13778075, Thermo Fisher) for the siRNA and LNAs. Bafilomycine A_1 (tlrl-baf1, InvivoGen) was diluted in DMSO to 100 µM and used at 50-100 nM for 4-6 hours. 4-thiouridine (T2933, Biomol) was used at 100 µM for 16 hours. For starvation, cells were washed twice with PBS and starved in low glucose DMEM lacking amino acids (D9800-13, USBiological) and serum.

RNA isolation and Northern blotting

RNA was isolated using TRI reagent (T9424, Sigma-Aldrich) as recommended by the manufacturer. RNA was dissolved in nuclease-free water and stored at -80°C. Typically, 10 or 15 µg of total RNA was mixed with 2x loading dye (95% formamide; 0.025% xylene cyanol and bromophenol blue; 18mM EDTA; 0.025% SDS), denatured for 5 min at 95°C, cooled on ice and loaded on 8% acrylamide (19:1), 7M urea polyacrylamide gels. A semi-dry blotting apparatus was used for blotting on Hybond N^+ membranes (RPN1520B, GE) which were UV auto-crosslinked, pre-hybridized for 1 hour at 50°C and used for hybridizations with ^{32}P labelled DNA

antisense oligonucleotide probes overnight at 50°C. The membranes were then washed three times with high stringency buffer (5X SSC; 5% SDS), three times with low stringency buffer (1X SSC; 1% SDS) and exposed to phosphorimaging screens for 4 hours or overnight. Screens were scanned at Typhoon FLA-7000 (GE) and TIFF images were quantifiied by ImageJ.

RNA interactome capture

RNA interactome capture was performed with minor modifications in the cell lysis procedure as previously described (S*1*). The cells were washed twice with PBS on ice before UV crosslinking at 150 mJ/cm^2. Cells were lysed directly with lysis buffer on the cell culture plates, scraped and lysates were sheared through a 27G needle before incubation with oligo d(T) beads (volume ratio lysate to beads 15:1) for 1 hour at 4°C. Beads were then washed twice with each wash buffer, and pooled eluates from three rounds of purification were used for RNAse treatment, concentration using Amicon 3K columns (UFC500396, Merck Millipore) and mixing with 4x sample buffer (4xSB) (200mM Tris-HCl pH6.8; 8% SDS; 40% Glycerol, 0.04% bromophenol blue, 400mM DTT; 10% beta mercaptoethanol) for SDS-PAGE.

RBDmap

RBDmap for HuH-7 cells was performed and analyzed as described (S*2*). The data can be accessed at http://www.hentze.embl.de/public/RBDmapHuH7.

Protein extracts, SDS-PAGE and Western blotting

For Western blotting, cells were washed twice with ice cold PBS on ice and lysed on plate using RIPA lysis buffer (89900, Thermo Fisher) supplemented with protease inhibitor (11873580001, Roche). Lysates were treated with benzonase (100U/ml, 71206, Merck Millipore) for 15 min on ice and the protein concentrations were measured. Lysates were mixed with 4xSB, boiled for 5 min and typically 15 µg of lysate was used for SDS-PAGE. Proteins were transferred to nitrocellulose or PVDF membranes using the Trans-Blot Turbo Transfer System (Bio-Rad) and blocked for 1 hour at room temperature with 5% milk in PBS; 0,05% Tween (PBS-T). Primary antibodies were incubated in 5% milk PBS-T either overnight at 4°C or 1 hour at RT, followed by 3x PBS-T washes, secondary antibody incubation in 5% milk in PBS-T for 1 hour at RT, 3x PBS-T washes and developed using ECL (WBKLS0500, Millipore). Antibodies used were anti-p62 (1:20 000; PM045, MBL; 1:20 000; H00008878-M01, Novus), TDP43 (1:10 000; 10782-2-AP, ProteinTech Group), β-actin (1:20 000; A5441, Sigma-Aldrich), LC3B (1:20 000; PM036, MBL) and GAPDH (1:20 000; G9545, Sigma-Aldrich). Secondary antibodies (goat anti-mouse IgG-HRP, sc-2005; goat anti-mouse IgG-HRP, sc-2004, Santa Cruz) were used at 1:20 000 dilution.

siRNA, LNAs

An siRNA pool targeting p62 (L-010230-00-0020, GE) was used at 30 nM concentration for 48 hours. As control siRNA an equimolar mix of Scramble (5' UUCUCCGAACGUGUCACGUtt 3'; s229174, Thermo Fisher), sLuciferase (5' CGGAUUACCAGGGAUUUCAtt 3'; Thermo Fisher) and SWNeg9 (5' UACGACCGGUCUAUCGUAGtt 3'; s444246, Thermo Fisher) was used. LNAs (Exiqon) targeting vtRNA1-1 (#1: 5' ttaaagaactgtcgaa 3'; #3: 5'ttaaagaactgtcga 3') and control negA (5' aacacgtctatacgc 3') were used at 25 or 50 nM for 48 hours.

Immunoprecipitations (IP)

0.75 µg of p62 antibody or appropriate control IgG was coupled for 1 hour at RT to 12.5 µl of Protein G coupled magnetic beads (10004D, Thermo Fisher). Cells were washed twice with cold PBS, lysed in lysis buffer (100mM NaCl; 50mM Tris-HCl pH7.5; 0.1% SDS; 1 mM $MgCl_2$; 0.1 mM $CaCl_2$; 1% NP40; 0.5% sodium deoxycholate; protease inhibitors (11873580001, Roche)) and homogenized by ultrasound (level 4, 3x 10sec, 50% amplitude) on ice. Lysates containing 2 mg of total protein were used for IP for 1 hour at 4°C, washed three times with high salt buffer (500mM NaCl; 20mM HEPES pH7.3; 1% NP-40; 0.1% SDS; 1 mM EDTA; 0.5% sodium deoxycholate; protease inhibitors (11873580001, Roche)) and three times with the lysis buffer. Proteins were eluted at low pH (0.1M glycin pH2.0) and neutralized with 0.2M Tris-HCl pH8.5.

Proteomics

In gel digestion. For in-gel processing, eluates from p62 and control IPs were separated by SDS-PAGE and stained with coomassie blue. Gel slices from the region around 60 kDa were cut from the gel and subjected to in-gel digestion with trypsin (S3). Subsequently, peptides were extracted from the gel pieces. Samples were sonicated for 15 minutes, centrifuged and the supernatant removed and placed in a clean tube. Subsequently, a solution of 50:50 water: acetonitrile, 1 % formic acid (2 x the volume of the gel pieces) was added and the samples were again sonicated for 15 minutes, centrifuged and the supernatant pooled with the first. The pooled supernatants were then dried down with the speed vacuum centrifuge. The samples were dissolved in 10 µL of reconstitution buffer (96:4 water: acetonitrile, 0.1% formic acid and analyzed by LC-MS/MS.

LC-MS/MS – Dionex LC. Peptides were separated using the UltiMate 3000 RSLC nano LC system (Dionex) fitted with a trapping (Dionex Acclaim PepMap100, 75 µm x 2 cm, C18, 3 µm, 100 Å) and an analytical column (Dionex Acclaim PepMap RSLC 75 µm x 15 cm C18, 2 µm, 100 Å). The outlet of the analytical column was coupled directly to a Q-Exactive (Thermo) using the proxeon nanoflow source in positive ion mode. Solvent A was water, 0.1 % formic acid and solvent B was acetonitrile, 0.1 % formic acid. The samples were loaded using the µLpickup mode of the autosampler, with a constant flow of solvent A at 6 µL/min onto the trapping column. Trapping time was 5 minutes. Peptides were eluted via the analytical column a constant flow of 0.3 µL/min. During the elution step, the percentage of solvent B increased in a linear fashion from 4 % to 7 % B in 5 minutes, then from 7 % to 25 % in a further 30 minutes and finally from 25 % to 40 % in another 5 minutes. Column cleaning at 85 % B followed,

lasting 5 minutes, before returning to initial conditions for the re-equilibration, lasting 10 minutes.

QE – MS - DDA. The peptides were introduced into the mass spectrometer (Q-Exactive, Thermo) via a Pico-Tip Emitter 360 µm OD x 20 µm ID; 10 µm tip (New Objective) and a spray voltage of 1.8 kV was applied. The capillary temperature was set at 250 °C. Full scan MS spectra with mass range 300-1500 m/z were acquired in profile mode in the FT with resolution of 70000. The filling time was set at maximum of 32 ms with a limitation of 1x106 ions. DDA was performed with the resolution of the Orbitrap set to 17500, with a fill time of 60 ms and a limitation of 5x105 ions. Normalized collision energy of 25 was used. A loop count of 15 with count 1 was used. Dynamic exclusion time of 30s was applied. An underfill ratio of 1%, corresponding to 8.3 x104 ions was used. The peptide match algorithm was set to 'off' and only charge states of 2+, 3+ and 4+ were selected for MS/MS. Isolation window was set to 2 m/z and 110 m/z set as the fixed first mass. MS/MS data was acquired in centroid mode. In order to improve the mass accuracy, a lock mass correction using a background ion (m/z 445.12003) was applied.

Polynucleotide kinase (PNK) assays

After homogenization the lysates were treated with 10 ng/µl of RNase A (R5503, Sigma-Aldrich) and 2U/ml Turbo DNAse (AM2238, Thermo Fisher) for 15 min at 37°C, cooled on ice and used for IPs. After the IP and washes, beads were washed additionally with PNK buffer (50mM NaCl; 50mM Tris-HCl pH7.5; 10mM MgCl2; 0.5% NP-40; protease inhibitors (11873580001, Roche)), then resuspended in PNK buffer containing 0.1 µCi/µl [γ-32P] rATP (Hartmann), 1 U/µl T4 PNK (NEB), 1mM DTT and labeled for 15 min at 37°C. After 4 washes with PNK buffer, proteins were eluted as described above, resolved by SDS-PAGE, blotted and membranes were exposed overnight to phosphorimager screens or to the imaging film (Z350397-50EA, Sigma), followed by Western blotting.

iCLIP

iCLIP was performed as published (S*4*) using IPs described above. Treatment of the lysates with RNAseI (AM2295, Thermo Fisher) was used at 20 U/ml.

Bioinformatics and statistical analyses

The analysis of the p62 iCLIP datasets is described at http://www.hentze.embl.de/public/p62-iCLIP. RNA secondary structures were predicted using the ViennaRNA package. Data are displayed as mean ± SEM, and two-tailed unpaired t test was used. Images were quantified with ImageJ.

Cloning

Full length human p62 wild type cDNA was cloned into pcDNA5_FRT/TO vector with N-terminal FLAG/HA tag (MDYKDDDDKSAGGYPYDVPDYAKL…) using HindIII and XhoI sites. Single and double amino acid mutations were done using PCR-mediated mutagenesis. Recognition sites of p62 siRNA were mutated in synonymous fashion (5' GGATCGAGGTAGACATAGA 3'; 5' GAGCAAATGGAATCCGACA 3'; 5' GGACGCACCTCTCATCTAA 3'; 5' CGACTGGCCTCAAAGAGGC 3'), cDNA was synthetized in pUC57 (GenScript) and swapped into p62 cDNA using BamHI and XhoI sites. Vault RNA with T7 or H1(2xTO) promotors were synthetized (GenScript) in pUC57 backbone.

In vitro transcription, RNA quantification and EMSA

pUC57 plasmid with T7_vault RNA1-1 was used for in vitro transcription reaction using MEGAshortscript kit (AM1354, Thermo Fisher) with ^{32}P-αUTP (SRP-210, Hartmann) according to the manufacturer's protocol. RNA was gel purified, phenol-chloroform extracted, dissolved in water and measured for the specific activity with scintillation counter and concentration with QuBit (Thermo Fisher). EMSA reactions containing 1 µM of proteins, 30 nM of RNA, 50 ng/µl of BSA and reaction buffer (50mM KCl; 10mM HEPES pH7.3; 0.25mM EDTA; 2,5mM MgCl2; 5%glycerol; 0.1% NP-40; 1mM DTT) were incubated 20 min at room temperature. After the reaction, heparin was added (final concentration 100 ng/µl) and samples were exposed to 10 min (corresponding to 1500 mJ/cm^2) of 254 nm UV-C light on ice. RNaseA (final concentration 100ng/µl) treatment was performed 15 min at 37°C where indicated. Samples were then mixed with 4xSB, incubated at 70°C for 10 min and analyzed by denaturing SDS-PAGE. Gel was dried for 1 hour at 80°C and exposed overnight to phosphorimager screen.

p62 protein expression and purification

MBP-p62-his$_6$ was expressed by autoinduction in ZY media for 16 hrs at 20°C. Cells were lysed by resuspension in lysis buffer (50mM HEPES pH 8.0, 1M NaCl, 0.5 mM TCEP, 1x protease inhibitor) followed by four passes through a microfluidizer. Lysate was clarified by centrifugation at 48 000 *g* and incubated with Ni-NTA beads for 1 hr. Beads were washed extensively in buffer 1 (50mM HEPES pH 8.0, 1M NaCl, 0.5 mM TCEP, 50mM Imidazole) and protein eluted with buffer 2 (50mM HEPES pH 8.0, 1M NaCl, 0.5 mM TCEP, 250mM Imidazole).

Immunofluorescence microscopy

For immunostaining, cells were cultured on ibidi slides (80426; ibidi), fixed for 10 min with 4 % paraformaldehyde, washed with PBS, permeabilized and blocked for 30 min in 0.1% Triton-X 100 in 1% BSA solution. Cells were then incubated with primary antibodies for 2 hours at room temperature, washed in PBS and incubated with the secondary antibody and DAPI for 1 h at room temperature in the dark. Slides were washed 3 times in PBS and stored at 4°C in PBS until imaging. Reagents used were anti-p62 1:500 (PM045, MBL), anti-LC3B 1:300 (CTB-LC3-2-IC, Cosmo Bio), anti-mouse IgG Alexa Fluor 488 1:1000 (4408, Cell Signaling), anti-Rabbit IgG

Alexa Fluor 555 1:1000 (4413, Cell Signaling), DAPI (10236276001 Roche). Fluorescent staining was viewed on a wide-field fluorescence microscope (Cellobserver HS; Carl Zeiss) equipped with a 63x Plan-Apochromat 1.4 oil objective and a Lumen Dznamics 120 LED light source. For detection of Dapi (Ex 353nm / Em 465nm), Alexa Fluor 488 (Ex 493nm / Em 517nm) and Alexa Fluor 555 (Ex 553nm / Em 568nm), the AxioCamMRm3 camera was used. Pictures were acquired using Zeiss software (ZEN 2 blue edition) and exported by ImageJ (version 2.0.0-rc-41/1.50d).

Sub-cellular fractionation

Cells were washed twice with PBS on ice before 254nm UV-C light exposure with 150 mJ/cm2. Cells were lysed directly on the plates with hypotonic buffer (10mM HEPES pH7.3; 20mM KCl; 1mM EDTA; 1% triton X-100; 1mM DTT; protease inhibitors (11873580001, Roche)) by swelling 10min on ice, followed by scraping. Lysates were homogenized by gentle pipetting and centrifuged for 10 min at 2.500xg at 4ºC. The nuclei/vesicles-containing pellet (P2.5) was carefully washed in hypotonic buffer, resuspended in extraction buffer (20mM HEPES pH7.3; 200mM NaCl; 5mM $MgCl_2$; 1% NP-40; protease inhibitors), sonicated, treated with 2U/ml Turbo DNase and RNaseA (see PNK assays procedure), salt content was adjusted by addition of 5xIP buffer (100mM HEPES pH7.3; 1M NaCl; 5mM EDTA; 5% NP-40; 0.5% SDS; 2.5% sodium deoxycholate; protease inhibitors) and samples were processed for IP. The supernatant (S2.5) was further centrifuged for 20 min at 20.000xg at 4ºC. The membrane debris containing pellet (P20) was resuspended in the extraction buffer, sonicated, treated with 2U/ml Turbo DNase and RNaseA, salt content was adjusted by addition of 5xIP buffer and samples were processed for IP. The supernatant (S20) was treated with 2U/ml Turbo DNase and RNaseA, salt content was adjusted by addition of 5xIP buffer and samples were processed for immunoprecipitation.

Supplementary Figures legend

Figure S1. Analysis of p62 RNA binding. (**A**) Stable HuH-7 cell clones expressing inducible FLAG/HA-tagged p62 wt and K141A variant were exposed to 254nm UV-C, lysed and IP with anti-HA antibody-conjugated beads and radioactive labeling was performed. The blot was exposed to phosphorimager screen and subsequently used for Western blotting. Endogenous and exogenous p62 are indicated by arrows. (**B**) Lysates from 254nm UV-C light exposed HuH-7 cells were treated with low (20U/ml RNaseI, L) or high concentration of RNase (200 U/ml, H), and used for IPs with indicated antibodies and controls. p62-RNA complexes were separated by SDS-PAGE, blotted and excised as indicated by the red dots rectangles. The underlined area of the blot was used for a subsequent Western blotting shown in panel (**C**). (**D**) Log_2 ratios of RNA enrichment in p62 IPs over the control IPs (Fisher exact test, *p-adj* < 0.05). (**E**) Cells were transfected with siRNA for 48 hours, then lysed and analyzed by Western blotting with the indicated antibodies. (**F**) Total RNA was isolated and analyzed by Northern blotting. vtRNA probe signals were quantified and normalized to the 5S rRNA, n=3.

Figure S2. p62 crosslink-sites (CS) analysis on vtRNAs. Significant (FDR 5%) CS read counts of p62 IPs displayed on the vtRNAs transcript sequence. RNA secondary structure is displayed next to the plot and nucleotides with CS mean count values above 5 are indicated in bold.

Figure S3. Overexpression and knock-down of vtRNAs. (**A**) Cells were transfected with plasmids expressing vault RNAs and lysed after 24 hours. Total RNA was isolated and analyzed by Northern blotting. (**B**) Cells were transfected with control LNA oligo (negA) or increasing amounts of LNA oligo targeting vtRNA1-1 and lysed after 48 hours. Total RNA was isolated and analyzed by Northern blotting.

Figure S4. Analysis of p62 localization and RNA binding. (**A**) HuH-7 cells were treated for 4 hours with BafA at 100nM, or starved for 4 hours in the presence of BafA at 100nM. Cells were then fixed with paraformaldehyde and stained with anti-p62 (red), anti-LC3B (green) and DAPI (blue). Representative images are shown; scale bars represent 20 μm. (**B**) Data of quantified RNA-bound p62/total p62 from Fig. 4B is plotted together with the total vtRNA1-1 levels acquired from the HuH-7 cells starved in minimal media for indicated time.

Supplementary references

S1. A. Castello *et al.*, System-wide identification of RNA-binding proteins by interactome capture. *Nature protocols* **8**, 491-500 (2013).

S2. A. Castello *et al.*, Comprehensive Identification of RNA-Binding Domains in Human Cells. *Molecular cell* **63**, 696-710 (2016).

S3. M. M. Savitski *et al.*, Tracking cancer drugs in living cells by thermal profiling of the proteome. *Science* **346**, 1255784 (2014).

S4. I. Huppertz *et al.*, iCLIP: protein-RNA interactions at nucleotide resolution. *Methods* **65**, 274-287 (2014).

Figure S1

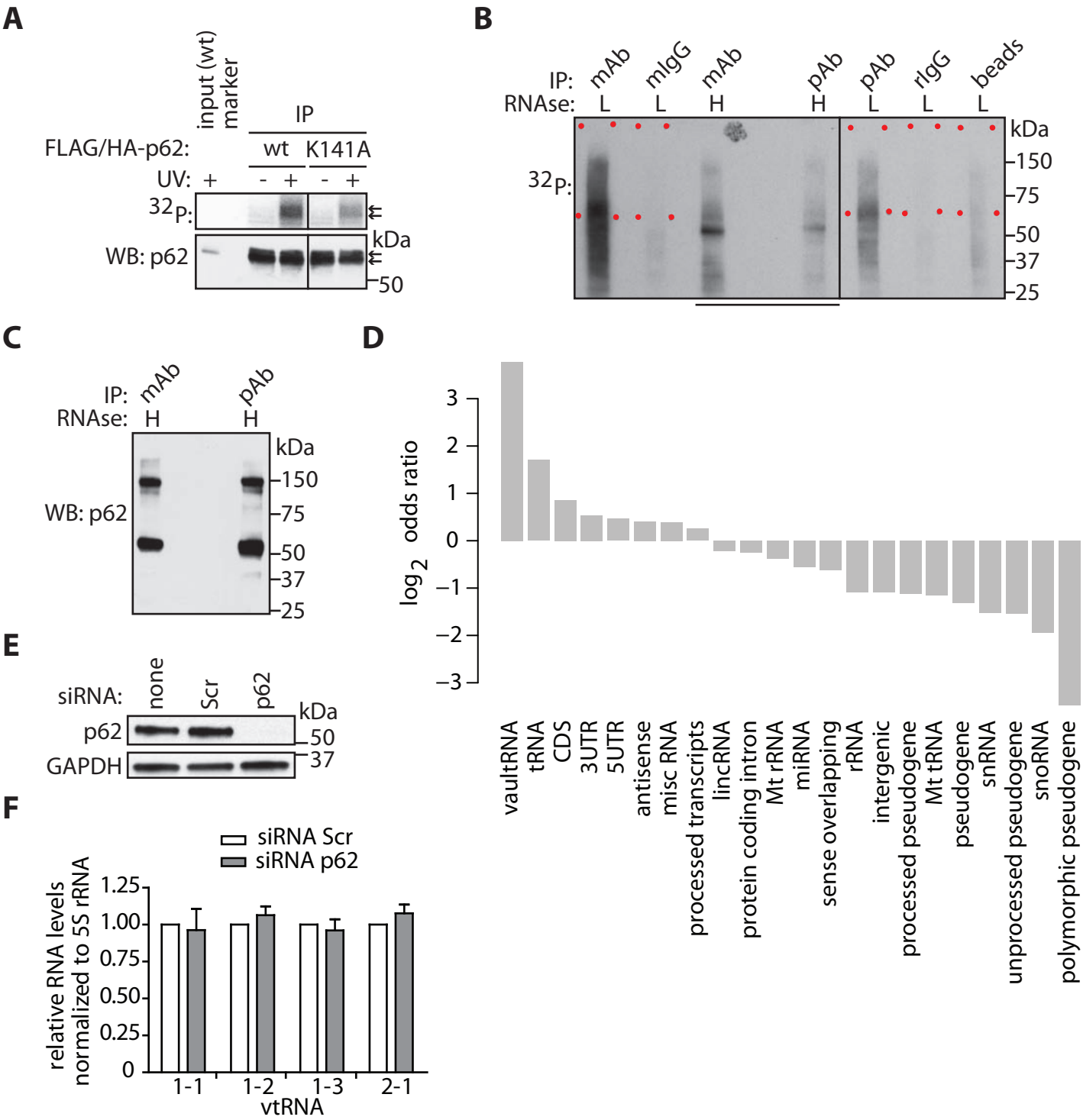

Figure S2

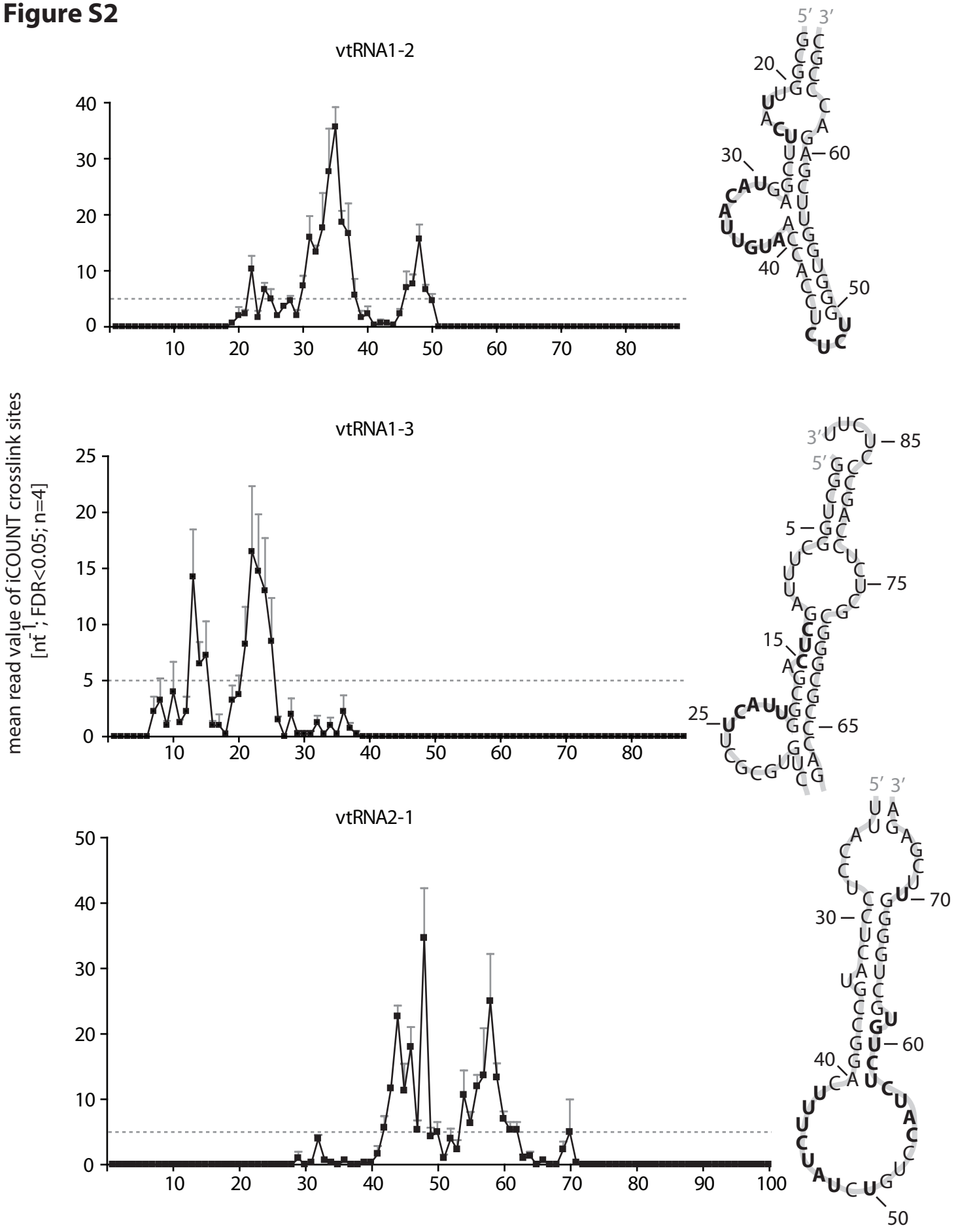

Figure S3

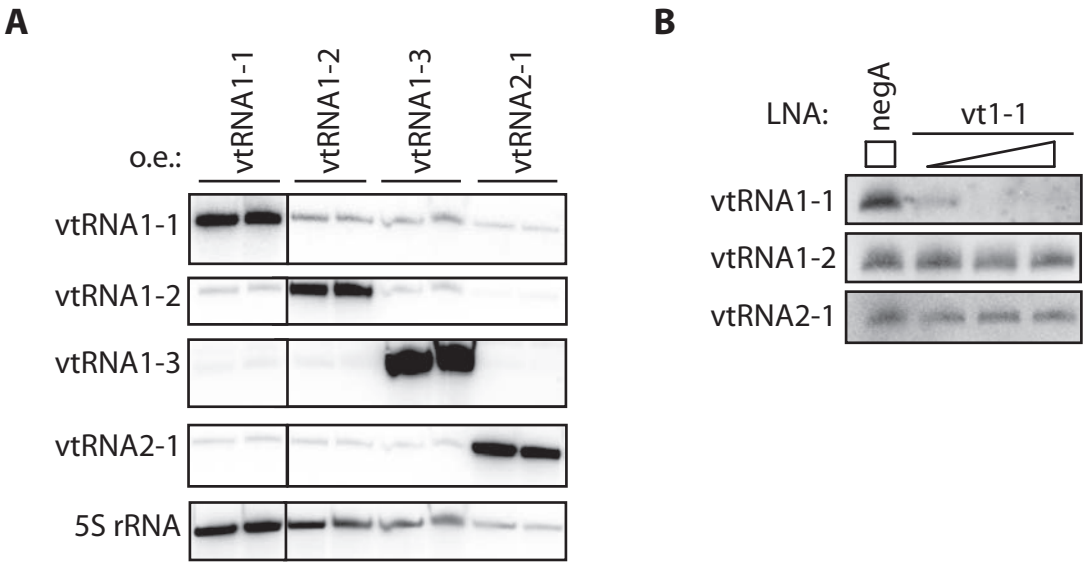

Figure S4

A

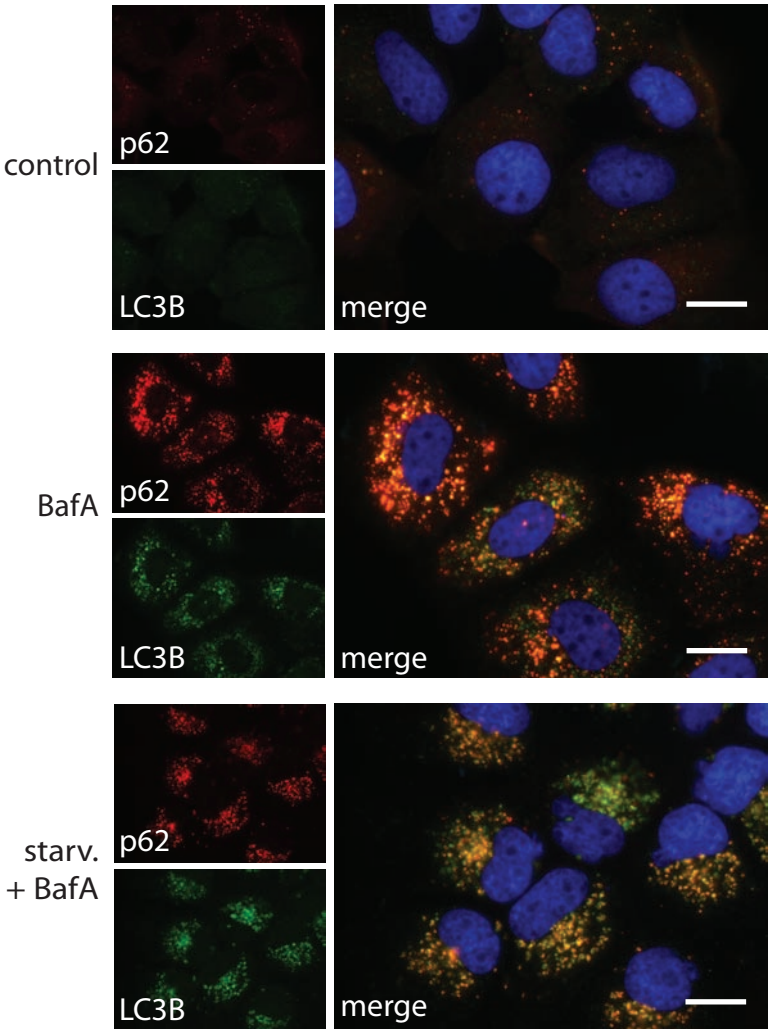

B

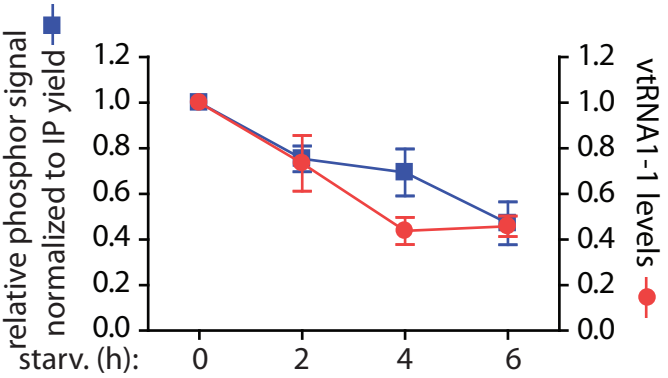

Table S1. This table lists the proteins found in the HuH-7 RBDmap.

ENSEMBL Gene ID	ENSEMBL Gene Name	Uniprot ID
ENSG00000148584	A1CF	Q9NQ94
ENSG00000144452	ABCA12	Q86UK0
ENSG00000075239	ACAT1	P24752
ENSG00000160710	ADAR	P55265
ENSG00000158467	AHCYL2	Q96HN2
ENSG00000124942	AHNAK	Q09666
ENSG00000105127	AKAP8	O43823
ENSG00000011243	AKAP8L	Q9ULX6
ENSG00000119711	ALDH6A1	Q02252
ENSG00000149925	ALDOA	P62861
ENSG00000091542	ALKBH5	Q6P6C2
ENSG00000183684	ALYREF	Q86V81
ENSG00000131503	ANKHD1	Q8IWZ3
ENSG00000182718	ANXA2	P07355
ENSG00000166181	API5	Q9BZZ5
ENSG00000021776	AQR	O60306
ENSG00000066777	ARFGEF1	Q9Y6D6
ENSG00000130429	ARPC1B	O15143
ENSG00000100325	ASCC2	Q9H1I8
ENSG00000163399	ATP1A1	P05023
ENSG00000152234	ATP5A1	P25705
ENSG00000204842	ATXN2	Q99700
ENSG00000168488	ATXN2L	Q8WWM7
ENSG00000165733	BMS1	Q14692
ENSG00000175573	C11orf68	Q9H3H3
ENSG00000130813	C19orf66	Q9NUL5
ENSG00000146540	C7orf50	Q9BRJ6
ENSG00000122786	CALD1	Q05682
ENSG00000178372	CALML5	Q9NZT1
ENSG00000135387	CAPRIN1	Q14444
ENSG00000121691	CAT	P04040
ENSG00000158941	CCAR2	Q8N163
ENSG00000180329	CCDC43	Q86WV7
ENSG00000105321	CCDC9	Q9Y3X0
ENSG00000096401	CDC5L	Q99459
ENSG00000149187	CELF1	Q92879
ENSG00000172757	CFL1	P23528
ENSG00000106554	CHCHD3	Q9NX63
ENSG00000100604	CHGA	P10645
ENSG00000160679	CHTOP	Q9Y3Y2
ENSG00000099622	CIRBP	Q14011
ENSG00000122873	CISD1	Q9NZ45
ENSG00000145354	CISD2	Q8N5K1
ENSG00000169714	CNBP	P62633
ENSG00000133313	CNDP2	Q96KP4
ENSG00000111596	CNOT2	Q9NZN8
ENSG00000168275	COA6	Q5JTJ3
ENSG00000187955	COL14A1	Q05707
ENSG00000181789	COPG1	Q9Y678
ENSG00000113742	CPEB4	Q17RY0
ENSG00000160917	CPSF4	O95639
ENSG00000149532	CPSF7	Q8N684
ENSG00000009307	CSDE1	O75534
ENSG00000141551	CSNK1D	P48730
ENSG00000159176	CSRP1	P21291
ENSG00000101811	CSTF2	P33240
ENSG00000115866	DARS	P14868
ENSG00000071626	DAZAP1	Q96EP5
ENSG00000155368	DBI	P07108
ENSG00000079785	DDX1	Q92499
ENSG00000100201	DDX17	Q92841
ENSG00000165732	DDX21	Q9NR30
ENSG00000215301	DDX3X	O00571
ENSG00000080007	DDX43	Q9NXZ2
ENSG00000108654	DDX5	P17844
ENSG00000107625	DDX50	Q9BQ39
ENSG00000141141	DDX52	Q9Y2R4
ENSG00000123064	DDX54	Q8TDD1
ENSG00000136271	DDX56	Q9NY93
ENSG00000110367	DDX6	P26196
ENSG00000109606	DHX15	O43143
ENSG00000067248	DHX29	Q7Z478
ENSG00000132153	DHX30	Q7L2E3
ENSG00000174953	DHX36	Q9H2U1
ENSG00000163214	DHX57	Q6P158
ENSG00000067596	DHX8	Q14562
ENSG00000135829	DHX9	Q08211
ENSG00000130826	DKC1	O60832
ENSG00000185842	DNAH14	Q0VDD8
ENSG00000086061	DNAJA1	P31689
ENSG00000128590	DNAJB9	Q9UBS3
ENSG00000136770	DNAJC1	Q96KC8
ENSG00000096696	DSP	P15924

ENSG00000133059	DSTYK	Q6XUX3
ENSG00000077380	DYNC1I2	Q13409
ENSG00000107223	EDF1	O60869
ENSG00000156508	EEF1A1	P68104
ENSG00000254772	EEF1G	B4DTG2
ENSG00000167658	EEF2	P13639
ENSG00000142634	EFHD2	Q96C19
ENSG00000107581	EIF3A	Q14152
ENSG00000106263	EIF3B	P55884
ENSG00000100353	EIF3D	O15371
ENSG00000130811	EIF3G	O75821
ENSG00000161960	EIF4A1	P60842
ENSG00000156976	EIF4A2	Q14240
ENSG00000063046	EIF4B	P23588
ENSG00000114867	EIF4G1	Q04637
ENSG00000110321	EIF4G2	P78344
ENSG00000106682	EIF4H	Q15056
ENSG00000158417	EIF5B	O60841
ENSG00000066044	ELAVL1	Q15717
ENSG00000143420	ENSA	O43768
ENSG00000136628	EPRS	P07814
ENSG00000103067	ESRP2	Q9H6T0
ENSG00000182944	EWSR1	Q01844
ENSG00000048828	FAM120A	Q9NZB2
ENSG00000184083	FAM120C	Q9NX05
ENSG00000172366	FAM195A	Q9BUT9
ENSG00000119812	FAM98A	Q8NCA5
ENSG00000164896	FASTK	Q14296
ENSG00000118246	FASTKD2	Q9NYY8
ENSG00000088832	FKBP1A	P62942
ENSG00000100442	FKBP3	Q00688
ENSG00000196924	FLNA	P21333
ENSG00000075420	FNDC3B	Q53EP0
ENSG00000151474	FRMD4A	Q9P2Q2
ENSG00000162613	FUBP1	Q96AE4
ENSG00000107164	FUBP3	Q96I24
ENSG00000089280	FUS	P35637
ENSG00000114416	FXR1	P51114
ENSG00000129245	FXR2	P51116
ENSG00000122068	FYTTD1	Q96QD9
ENSG00000145907	G3BP1	Q13283
ENSG00000138757	G3BP2	Q9UN86
ENSG00000089154	GCN1L1	Q92616
ENSG00000204628	GNB2L1	P63244
ENSG00000130119	GNL3L	Q9NVN8
ENSG00000143147	GPR161	Q8N6U8

ENSG00000132463	GRSF1	Q12849
ENSG00000105447	GRWD1	Q9BQ67
ENSG00000103342	GSPT1	P15170
ENSG00000189060	H1F0	P07305
ENSG00000113648	H2AFY	O75367
ENSG00000115677	HDLBP	Q00341
ENSG00000106049	HIBADH	P31937
ENSG00000184357	HIST1H1B	P16401
ENSG00000187837	HIST1H1C	P16403
ENSG00000168298	HIST1H1E	P10412
ENSG00000124529	HIST1H4B	P62805
ENSG00000189403	HMGB1	P09429
ENSG00000164104	HMGB2	P26583
ENSG00000177733	HNRNPA0	Q13151
ENSG00000135486	HNRNPA1	P09651
ENSG00000122566	HNRNPA2B1	P22626
ENSG00000170144	HNRNPA3	P51991
ENSG00000197451	HNRNPAB	Q99729
ENSG00000092199	HNRNPC	P07910
ENSG00000179172	HNRNPCL1	O60812
ENSG00000138668	HNRNPD	Q14103
ENSG00000152795	HNRNPDL	O14979
ENSG00000169813	HNRNPF	P52597
ENSG00000169045	HNRNPH1	P31943
ENSG00000126945	HNRNPH2	P55795
ENSG00000096746	HNRNPH3	P31942
ENSG00000165119	HNRNPK	P61978
ENSG00000104824	HNRNPL	P14866
ENSG00000143889	HNRNPLL	Q8WVV9
ENSG00000099783	HNRNPM	P52272
ENSG00000125944	HNRNPR	O43390
ENSG00000153187	HNRNPU	Q00839
ENSG00000105323	HNRNPUL1	Q9BUJ2
ENSG00000132541	HRSP12	P52758
ENSG00000080824	HSP90AA1	P07900
ENSG00000096384	HSP90AB1	P08238
ENSG00000044574	HSPA5	P11021
ENSG00000159217	IGF2BP1	Q9NZI8
ENSG00000073792	IGF2BP2	Q9Y6M1
ENSG00000136231	IGF2BP3	O00425
ENSG00000211896	IGHG1	P01857
ENSG00000143621	ILF2	Q12905
ENSG00000129351	ILF3	Q12906
ENSG00000140575	IQGAP1	P46940
ENSG00000163207	IVL	P07476
ENSG00000173801	JUP	P14923

ENSG00000121774	KHDRBS1	Q07666
ENSG00000131773	KHDRBS3	O75525
ENSG00000088247	KHSRP	Q92945
ENSG00000129250	KIF1C	O43896
ENSG00000155506	LARP1	Q6PKG0
ENSG00000161813	LARP4	Q71RC2
ENSG00000107929	LARP4B	Q92615
ENSG00000002834	LASP1	Q14847
ENSG00000111716	LDHB	P07195
ENSG00000168924	LETM1	O95202
ENSG00000178934	LGALS7B	P47929
ENSG00000187772	LIN28B	Q6ZN17
ENSG00000138095	LRPPRC	P42704
ENSG00000130764	LRRC47	Q8N1G4
ENSG00000108829	LRRC59	Q96AG4
ENSG00000257103	LSM14A	Q8ND56
ENSG00000149657	LSM14B	Q9BX40
ENSG00000145220	LYAR	Q9NX58
ENSG00000145050	MANF	P55145
ENSG00000131711	MAP1B	P46821
ENSG00000078018	MAP2	P11137
ENSG00000047849	MAP4	P27816
ENSG00000015479	MATR3	P43243
ENSG00000146701	MDH2	P40926
ENSG00000169057	MECP2	P51608
ENSG00000254726	MEX3A	A1L020
ENSG00000176624	MEX3C	Q5U5Q3
ENSG00000181588	MEX3D	Q86XN8
ENSG00000148773	MKI67	P46013
ENSG00000075975	MKRN2	Q9H000
ENSG00000179455	MKRN3	Q13064
ENSG00000155363	MOV10	Q9HCE1
ENSG00000174547	MRPL11	Q9Y3B7
ENSG00000172172	MRPL13	Q9BYD1
ENSG00000082515	MRPL22	Q9NWU5
ENSG00000108826	MRPL27	Q9P0M9
ENSG00000130312	MRPL34	Q9BQ48
ENSG00000181610	MRPS23	Q9Y3D9
ENSG00000062582	MRPS24	Q96EL2
ENSG00000125445	MRPS7	Q9Y2R9
ENSG00000135097	MSI1	O43347
ENSG00000153944	MSI2	Q96DH6
ENSG00000147065	MSN	P26038
ENSG00000100714	MTHFD1	P11586
ENSG00000103248	MTHFSD	Q2M296
ENSG00000107951	MTPAP	Q9NVV4

ENSG00000132382	MYBBP1A	Q9BQG0
ENSG00000115053	NCL	P19338
ENSG00000155438	NIFK	Q9BYG3
ENSG00000239672	NME1	P15531
ENSG00000173145	NOC3L	Q8WTT2
ENSG00000147140	NONO	Q15233
ENSG00000111641	NOP2	P46087
ENSG00000196943	NOP9	Q86U38
ENSG00000181163	NPM1	P06748
ENSG00000130305	NSUN5	Q96P11
ENSG00000167005	NUDT21	O43809
ENSG00000136243	NUPL2	O15504
ENSG00000162231	NXF1	Q9UBU9
ENSG00000185624	P4HB	P07237
ENSG00000070756	PABPC1	P11940
ENSG00000090621	PABPC4	Q13310
ENSG00000100836	PABPN1	Q86U42
ENSG00000059378	PARP12	Q9H0J9
ENSG00000166889	PATL1	Q86TB9
ENSG00000177425	PAWR	Q96IZ0
ENSG00000169564	PCBP1	Q15365
ENSG00000197111	PCBP2	Q15366
ENSG00000090097	PCBP4	P57723
ENSG00000106244	PDAP1	Q13442
ENSG00000148843	PDCD11	Q14690
ENSG00000167004	PDIA3	P30101
ENSG00000163110	PDLIM5	Q96HC4
ENSG00000121892	PDS5A	Q29RF7
ENSG00000089220	PEBP1	P30086
ENSG00000242265	PEG10	Q86TG7
ENSG00000100410	PHF5A	Q7RTV0
ENSG00000092621	PHGDH	O43175
ENSG00000067225	PKM	P14618
ENSG00000100227	POLDIP3	Q9BY77
ENSG00000099821	POLRMT	O00411
ENSG00000131013	PPIL4	Q8WUA2
ENSG00000204569	PPP1R10	Q96QC0
ENSG00000204619	PPP1R11	O60927
ENSG00000123131	PRDX4	Q13162
ENSG00000253729	PRKDC	P78527
ENSG00000147471	PROSC	O94903
ENSG00000174231	PRPF8	Q6P2Q9
ENSG00000204469	PRRC2A	P48634
ENSG00000117523	PRRC2C	Q9Y520
ENSG00000159352	PSMD4	P55036
ENSG00000121390	PSPC1	Q8WXF1

ENSG00000011304	PTBP1	P26599
ENSG00000119314	PTBP3	O95758
ENSG00000179950	PUF60	Q9UHX1
ENSG00000134644	PUM1	Q14671
ENSG00000055917	PUM2	Q8TB72
ENSG00000185129	PURA	Q00577
ENSG00000146676	PURB	Q96QR8
ENSG00000048991	R3HDM1	Q15032
ENSG00000179912	R3HDM2	Q9Y2K5
ENSG00000125970	RALY	Q9UKM9
ENSG00000132341	RAN	P62826
ENSG00000132359	RAP1GAP2	Q684P5
ENSG00000117222	RBBP5	Q15291
ENSG00000182872	RBM10	P98175
ENSG00000183808	RBM12B	Q8IXT5
ENSG00000239306	RBM14	Q96PK6
ENSG00000162775	RBM15	Q96T37
ENSG00000179837	RBM15B	Q8NDT2
ENSG00000122965	RBM19	Q9Y4C8
ENSG00000086589	RBM22	Q9NW64
ENSG00000112183	RBM24	Q9BX46
ENSG00000119707	RBM25	P49756
ENSG00000091009	RBM27	Q9P2N5
ENSG00000106344	RBM28	Q9NW13
ENSG00000102317	RBM3	P98179
ENSG00000184863	RBM33	Q96EV2
ENSG00000188739	RBM34	P42696
ENSG00000132819	RBM38	Q9H0Z9
ENSG00000131051	RBM39	Q14498
ENSG00000173933	RBM4	Q9BWF3
ENSG00000155636	RBM45	Q8IUH3
ENSG00000163694	RBM47	A0AV96
ENSG00000173914	RBM4B	Q9BQ04
ENSG00000003756	RBM5	P52756
ENSG00000004534	RBM6	P78332
ENSG00000153250	RBMS1	P29558
ENSG00000076067	RBMS2	Q15434
ENSG00000147274	RBMX	P38159
ENSG00000134597	RBMX2	Q9Y388
ENSG00000213516	RBMXL1	Q96E39
ENSG00000157110	RBPMS	Q93062
ENSG00000135870	RC3H1	Q5TC82
ENSG00000023191	RNH1	P13489
ENSG00000198755	RPL10A	P62906
ENSG00000167526	RPL13	P26373
ENSG00000142541	RPL13A	P40429

ENSG00000188846	RPL14	P50914
ENSG00000174748	RPL15	P61313
ENSG00000265681	RPL17	P18621
ENSG00000105640	RPL18A	Q02543
ENSG00000122026	RPL21	P46778
ENSG00000125691	RPL23	P62829
ENSG00000114391	RPL24	P83731
ENSG00000166441	RPL27A	P46776
ENSG00000108107	RPL28	P46779
ENSG00000100316	RPL3	P39023
ENSG00000071082	RPL31	P62899
ENSG00000144713	RPL32	P62910
ENSG00000130255	RPL36	Q9Y3U8
ENSG00000172809	RPL38	P63173
ENSG00000174444	RPL4	P36578
ENSG00000089009	RPL6	Q02878
ENSG00000147604	RPL7	P18124
ENSG00000148303	RPL7A	P62424
ENSG00000161016	RPL8	P62917
ENSG00000177600	RPLP2	P05387
ENSG00000163902	RPN1	P04843
ENSG00000124614	RPS10	P46783
ENSG00000142534	RPS11	P62280
ENSG00000112306	RPS12	P25398
ENSG00000110700	RPS13	P62277
ENSG00000164587	RPS14	P62263
ENSG00000105193	RPS16	P62249
ENSG00000105372	RPS19	P39019
ENSG00000187051	RPS19BP1	Q86WX3
ENSG00000140988	RPS2	P15880
ENSG00000008988	RPS20	P60866
ENSG00000138326	RPS24	P62847
ENSG00000118181	RPS25	P62851
ENSG00000197728	RPS26	P62854
ENSG00000177954	RPS27	P42677
ENSG00000233927	RPS28	P62857
ENSG00000149273	RPS3	P23396
ENSG00000145425	RPS3A	P61247
ENSG00000198034	RPS4X	P62701
ENSG00000083845	RPS5	P46782
ENSG00000137154	RPS6	P62753
ENSG00000171863	RPS7	P62081
ENSG00000142937	RPS8	P62241
ENSG00000156990	RPUSD3	Q6P087
ENSG00000052749	RRP12	Q5JTH9
ENSG00000132275	RRP8	O43159

ENSG00000179041	RRS1	Q15050
ENSG00000171490	RSL1D1	O76021
ENSG00000100220	RTCB	Q9Y3I0
ENSG00000182552	RWDD4	Q6NW29
ENSG00000163220	S100A9	P06702
ENSG00000160633	SAFB	Q15424
ENSG00000031698	SARS	P49591
ENSG00000126524	SBDS	Q9Y3A5
ENSG00000138758	Sep 11	Q9NVA2
ENSG00000142864	SERBP1	Q8NC51
ENSG00000206075	SERPINB5	P36952
ENSG00000168066	SF1	Q15637
ENSG00000115524	SF3B1	O75533
ENSG00000143368	SF3B4	Q15427
ENSG00000116560	SFPQ	P23246
ENSG00000145832	SLC25A48	Q6ZT89
ENSG00000022567	SLC45A4	Q5BKX6
ENSG00000119705	SLIRP	Q9GZT3
ENSG00000137776	SLTM	Q9NWH9
ENSG00000198887	SMC5	Q8IY18
ENSG00000197157	SND1	Q7KZF4
ENSG00000131876	SNRPA1	P09661
ENSG00000167088	SNRPD1	P62314
ENSG00000125743	SNRPD2	P62316
ENSG00000100028	SNRPD3	P62318
ENSG00000182004	SNRPE	P62304
ENSG00000143977	SNRPG	P62308
ENSG00000172164	SNTB1	Q13884
ENSG00000168807	SNTB2	Q13425
ENSG00000095637	SORBS1	Q9BX66
ENSG00000123352	SPATS2	Q86XZ4
ENSG00000196141	SPATS2L	Q9NUQ6
ENSG00000065526	SPEN	Q96T58
ENSG00000197694	SPTAN1	Q13813
ENSG00000137877	SPTBN5	Q9NRC6
ENSG00000161011	SQSTM1	Q13501
ENSG00000068784	SRBD1	Q8N5C6
ENSG00000174780	SRP72	O76094
ENSG00000144867	SRPRB	Q9Y5M8
ENSG00000167978	SRRM2	Q9UQ35
ENSG00000087087	SRRT	Q9BXP5
ENSG00000136450	SRSF1	Q07955
ENSG00000188529	SRSF10	O75494
ENSG00000154548	SRSF12	Q8WXF0
ENSG00000161547	SRSF2	Q01130
ENSG00000112081	SRSF3	P84103

ENSG00000100650	SRSF5	Q13243
ENSG00000124193	SRSF6	Q13247
ENSG00000115875	SRSF7	Q16629
ENSG00000111786	SRSF9	Q13242
ENSG00000138385	SSB	P05455
ENSG00000106028	SSBP1	Q04837
ENSG00000100380	ST13	P50502
ENSG00000124214	STAU1	O95793
ENSG00000040341	STAU2	Q9NUL3
ENSG00000064607	SUGP2	Q8IX01
ENSG00000135316	SYNCRIP	O60506
ENSG00000136463	TACO1	Q9BSH4
ENSG00000172660	TAF15	Q92804
ENSG00000149591	TAGLN	Q01995
ENSG00000158710	TAGLN2	P37802
ENSG00000120948	TARDBP	Q13148
ENSG00000136270	TBRG4	Q969Z0
ENSG00000187735	TCEA1	P23193
ENSG00000116001	TIA1	P31483
ENSG00000151923	TIAL1	Q01085
ENSG00000164548	TRA2A	Q13595
ENSG00000136527	TRA2B	P62995
ENSG00000206557	TRIM71	Q2Q1W2
ENSG00000174173	TRMT10C	Q7L0Y3
ENSG00000180098	TRNAU1AP	Q9NX07
ENSG00000167112	TRUB2	O95900
ENSG00000127824	TUBA4A	P68366
ENSG00000160201	U2AF1	Q01081
ENSG00000063244	U2AF2	P26368
ENSG00000143569	UBAP2L	Q14157
ENSG00000130725	UBE2M	P61081
ENSG00000135018	UBQLN1	Q9UMX0
ENSG00000116750	UCHL5	Q9Y5K5
ENSG00000005007	UPF1	Q92900
ENSG00000165280	VCP	P55072
ENSG00000026025	VIM	P08670
ENSG00000115368	WDR75	Q8IWA0
ENSG00000079246	XRCC5	P13010
ENSG00000196419	XRCC6	P12956
ENSG00000088930	XRN2	Q9H0D6
ENSG00000065978	YBX1	P67809
ENSG00000060138	YBX3	P16989
ENSG00000047188	YTHDC2	Q9H6S0
ENSG00000149658	YTHDF1	Q9BYJ9
ENSG00000198492	YTHDF2	Q9Y5A9
ENSG00000170027	YWHAG	P61981

ENSG00000122299	ZC3H7A	Q8IWR0
ENSG00000100403	ZC3H7B	Q9UGR2
ENSG00000105939	ZC3HAV1	Q7Z2W4
ENSG00000134744	ZCCHC11	Q5TAX3
ENSG00000177764	ZCCHC3	Q9NUD5

ENSG00000152518	ZFP36L2	P47974
ENSG00000056097	ZFR	Q96KR1
ENSG00000162664	ZNF326	Q5BKZ1
ENSG00000167962	ZNF598	Q86UK7

Table S2

Proteomics analysis of IP eluates after control (IgG) or polyclonal rabbit p62 antibody pulldown excised from SDS-PAGE gel around 60 kDa MW.

IgG

Accession #	Protein	Scores	Peptides	Sequence coverage [%]
I3L3I4	Actin, cytoplasmic 2, N-terminally processed OS=Homo sapiens GN=ACTG1 PE=4 SV=1	181,7	5	13.1
P62805	Histone H4 OS=Homo sapiens GN=HIST1H4A PE=1 SV=2	158,2	3	29.1
P01857	Ig gamma-1 chain C region OS=Homo sapiens GN=IGHG1 PE=1 SV=1	146,6	4	5.8
F8VU64	Keratin, type II cytoskeletal 8 OS=Homo sapiens GN=KRT8 PE=4 SV=1	138,2	2	8.8

Rabbit p62 pAb

Accession #	Protein	Scores	Peptides	Sequence coverage [%]
Q13501	Sequestosome-1 OS=Homo sapiens GN=SQSTM1 PE=1 SV=1	**1393,5**	17	**49.5**
Q13501-2	Isoform 2 of Sequestosome-1 OS=Homo sapiens GN=SQSTM1	**1356,3**	2	**56.2**
Q14145	Kelch-like ECH-associated protein 1 OS=Homo sapiens GN=KEAP1 PE=1 SV=2	1209,9	21	27.9
Q6UYC3	Lamin A/C OS=Homo sapiens GN=LMNA PE=2 SV=1	1089,3	20	32.1
P15924	Desmoplakin OS=Homo sapiens GN=DSP PE=1 SV=3	552,7	13	4.1
P08670	Vimentin OS=Homo sapiens GN=VIM PE=1 SV=4	490	10	25.8
G5E9V1	Protein TFG OS=Homo sapiens GN=TFG PE=4 SV=1	464,7	9	23.2
P14923	Junction plakoglobin OS=Homo sapiens GN=JUP PE=1 SV=3	276,7	4	7.4
F5GYZ3	Non-POU domain-containing octamer-binding protein OS=Homo sapiens GN=NONO PE=4 SV=1	269,3	6	16.0
B4DW52	Actin, cytoplasmic 1, N-terminally processed OS=Homo sapiens GN=ACTB PE=2 SV=1	216,9	4	11.0
Q96GM5	SWI/SNF-related matrix-associated actin-dependent regulator of chromatin subfamily D member 1 OS=Homo sapiens GN=SMARCD1 PE=1 SV=2	212,5	6	11.3
P62979	Ubiquitin-40S ribosomal protein S27a OS=Homo sapiens GN=RPS27A PE=1 SV=2	199,9	4	28.2
B4DEB1	Histone H3 OS=Homo sapiens GN=H3F3A PE=2 SV=1	182,8	5	26.8
P17987	T-complex protein 1 subunit alpha OS=Homo sapiens GN=TCP1 PE=1 SV=1	178,9	5	9.2

Table S2 (continued)

Accession	Protein	Scores	Peptides	Sequence coverage [%]
Q02413	Desmoglein-1 OS=Homo sapiens GN=DSG1 PE=1 SV=2	148,3	4	4.6
P62805	Histone H4 OS=Homo sapiens GN=HIST1H4A PE=1 SV=2	143,9	3	29.1
A6NIT8	Heterogeneous nuclear ribonucleoprotein L OS=Homo sapiens GN=HNRNPL PE=2 SV=1	133,9	3	6.8
Q5JW30	Double-stranded RNA-binding protein Staufen homolog 1 OS=Homo sapiens GN=STAU1 PE=2 SV=1	127,9	4	10.3
G3V3V0	Putative Polycomb group protein ASXL1 (Fragment) OS=Homo sapiens GN=ASXL1 PE=4 SV=1	120,4	3	12.5
H0YEM1	Poly(U)-binding-splicing factor PUF60 (Fragment) OS=Homo sapiens GN=PUF60 PE=4 SV=1	103,7	3	10.4
P81605	Dermcidin OS=Homo sapiens GN=DCD PE=1 SV=2	100,1	2	22.7

Table S3

Crosslink sites per RNA type, length and library size normalized.
M…Mouse R…Rabbit A / B … Batches
pAb – polyclonal antibody, mAb – monoclonal antibody

	Total length	Rabbit pAb -B	Rabbit pAb -A	Mouse mAb-A	Mouse mAb - B	Empty beads- A	Empty beads- B	IgG-M- A	IgG-M- B	IgG-R- A	IgG-R- B
vaultRNA	377	**51497,73**	**56495,53**	**45851,25**	**63375,86**	2954,18	10971,78	4922,89	4814,80	1630,78	1243,00
tRNAscan	45214	9759,71	6495,51	9245,27	13042,38	2863,51	4116,78	1866,69	3378,99	1998,86	4425,55
Mt_rRNA	2513	3862,84	4454,75	7803,30	4599,45	5983,02	5102,55	7420,48	7825,09	5137,65	5407,76
Mt_tRNA	1508	802,72	1197,35	3034,74	1002,62	2954,18	3017,24	3106,11	2206,78	3941,06	3107,50
rRNA	59444	129,23	56,66	282,02	114,46	231,07	507,96	127,86	386,79	113,77	654,31
misc_RNA	426141	35,02	39,41	34,78	33,43	28,53	34,94	19,49	24,85	41,84	37,39
snRNA	207473	25,47	20,96	39,09	25,70	72,92	59,81	47,28	113,74	98,78	101,64
miRNA	269361	20,22	13,60	21,39	29,76	23,09	49,14	23,62	44,93	23,59	31,31
3UTR	27069668	2,99	4,86	3,74	3,77	2,79	2,55	3,36	2,94	2,66	1,63
5UTR	25804825	2,98	4,84	3,80	3,79	3,18	2,42	3,46	2,88	2,53	2,11
CDS	28815147	2,67	4,56	3,57	3,53	2,00	2,01	2,38	2,86	1,69	2,07
protein_coding_exon	16764974	1,35	1,60	1,25	1,21	1,33	0,94	1,58	1,21	1,22	0,67
snoRNA	163910	1,14	2,79	3,18	1,82	9,06	12,62	11,32	5,54	8,75	2,86
transcribed_unitary_pseudogene	28235	0,82	0,00	1,68	0,00	0,00	0,00	0,00	0,00	0,00	0,00
macro_lncRNA	205012	0,79	1,44	1,97	0,68	0,91	0,00	1,29	1,48	7,00	0,00
processed_pseudogene	8047388	0,58	1,18	1,05	1,07	1,22	1,03	0,90	1,58	0,87	1,34
processed_transcript	25693208	0,56	0,50	0,44	0,51	0,35	0,64	0,38	0,51	0,54	0,35
protein_coding_intron	1229641747	0,50	0,50	0,45	0,35	0,57	0,49	0,59	0,52	0,57	0,43
antisense	116193196	0,41	0,37	0,37	0,40	0,29	0,27	0,31	0,25	0,25	0,30
sense_overlapping	6952261	0,28	0,27	0,28	0,15	0,20	0,54	0,32	0,48	0,44	1,21
transcribed_processed_pseudogene	4749013	0,26	0,24	0,27	0,16	0,57	0,44	0,35	0,57	0,65	0,69
3prime_overlapping_ncrna	194829	0,24	0,38	0,37	0,20	0,00	2,12	1,81	0,00	0,00	0,00

TEC	1757413	0,24	0,17	0,16	0,17	0,21	0,00	0,10	0,17	0,35	0,00
lincRNA	217616266	0,23	0,22	0,23	0,20	0,26	0,19	0,25	0,25	0,30	0,28
transcribed_unprocessed_pseudogene	15883155	0,22	0,23	0,20	0,17	0,25	0,29	0,28	0,23	0,26	0,09
unitary_pseudogene	4077426	0,21	0,20	0,20	0,18	0,18	0,20	0,20	0,00	0,25	0,11
polymorphic_pseudogene	572666	0,08	0,06	0,00	0,00	0,32	0,00	0,46	0,00	1,79	0,00
unprocessed_pseudogene	12920475	0,06	0,06	0,07	0,04	0,19	0,19	0,11	0,19	0,13	0,36
sense_intronic	4990054	0,05	0,06	0,09	0,06	0,02	0,08	0,04	0,00	0,08	0,00
pseudogene	3547420	0,02	0,05	0,07	0,06	0,37	0,12	0,00	0,00	0,00	0,00
IG_C_pseudogene	9112	0,00	0,00	0,00	0,00	0,00	0,00	0,00	0,00	0,00	0,00
IG_D_gene	851	0,00	0,00	0,00	0,00	0,00	0,00	0,00	0,00	0,00	0,00
IG_J_gene	1198	0,00	0,00	0,00	0,00	0,00	0,00	0,00	0,00	0,00	0,00
IG_J_pseudogene	165	0,00	0,00	0,00	0,00	0,00	0,00	0,00	0,00	0,00	0,00
IG_V_pseudogene	69688	0,00	0,00	0,00	0,00	0,00	0,00	0,00	0,00	0,00	0,00
translated_unprocessed_pseudogene	44659	0,00	0,00	0,00	0,00	0,00	0,00	0,00	0,00	0,00	0,00
TR_D_gene	39	0,00	0,00	0,00	0,00	0,00	0,00	0,00	0,00	0,00	0,00
TR_J_gene	4308	0,00	0,00	0,00	0,00	0,00	0,00	0,00	0,00	0,00	0,00
TR_J_pseudogene	299	0,00	0,00	0,00	0,00	0,00	0,00	0,00	0,00	0,00	0,00
TR_V_gene	61855	0,00	0,00	0,00	0,00	0,00	0,00	0,00	0,00	0,00	0,00
TR_V_pseudogene	13064	0,00	0,00	0,00	0,00	0,00	0,00	0,00	0,00	0,00	0,00
vaultRNA_pseudogene	102	0,00	0,00	0,00	0,00	0,00	0,00	0,00	0,00	0,00	0,00
TR_C_gene	638633	0,00	0,00	0,04	0,00	0,00	0,00	0,00	0,00	0,00	0,00
IG_C_gene	1898345	0,00	0,00	0,00	0,01	0,00	0,00	0,00	0,00	0,00	0,00
IG_V_gene	441901	0,00	0,00	0,05	0,05	0,00	0,00	0,00	0,00	0,00	0,00